CEAS Space Journal
https://doi.org/10.1007/s12567-023-00514-y

ORIGINAL PAPER

Experimental demonstration of a method to actively stabilize satellite structures against random perturbations of thermal boundary conditions using a closed-loop filter and controller approach

F. Möller[1] · T. Essig[1] · S. Holzhauer[1] · R. Förstner[1]

Received: 7 March 2023 / Revised: 28 June 2023 / Accepted: 30 June 2023

Abstract
Modern space travel requires increasingly stable support structures for optical instruments or antennas, which can hardly be realized with the traditional approaches. Therefore, an approach for active structural stabilization of thermal-induced distortions was developed, simulated, and patented within the framework of the Infrared Astronomy Satellite Swarm Interferometry (IRASSI) project. Based on this approach, the thermomechanical transfer functions between the change in heat flux and the change in displacement of the finite-element (FE) model of a structure have already been validated in their basic functionality. In an experimental setup, the FE model was extended to include a closed-loop filter and controller approach consisting of a Kalman filter processing the temperature measurements in conjunction with a Linear Quadratic Regulator (LQR). It was shown that this setup can compensate for predefined sinusoidally oscillating disturbance heat flows, with an improvement of 4 dB compared to the uncontrolled case. In this paper, an experimental setup revised with respect to the positioning of the sensors and control heating elements, in conjunction with an extension of the filter and controller approach, will demonstrate that the system can respond to reproducible, random fluctuations in the disturbance heat flux, as well as stepped changes, and that performance has improved due to the revision.

Keywords Structural stability · Active structural stabilization · Thermomechanical transfer function · Smart structures

Abbreviations

DASYLab	Data acquisition system laboratory
DIC	Digital image correlation
FEM	Finite-element method
IRASSI	Infrared astronomy satellite swarm interferometry
LQR	Linear quadratic regulator
PCU	Process cooling unit
PTFE	Polytetrafluorethylen
TVC	Thermal vacuum chamber

1 Introduction

The precise alignment of optical instruments or antennas on a satellite platform requires structural stability that can no longer be adequately provided by the conventional, passive methods, such as the use of materials with high stiffness and low coefficients of thermal expansion. As part of the IRASSI (InfraRed Astronomy Satellite Swarm Interferometry) project, an approach to actively stabilize structures against low-frequency periodic heat-induced distortions has been developed, simulated, and patented [1, 2].

In this work, an FE model based on this approach is experimentally validated. For this purpose, an experimental setup consisting of an aluminum plate with 18 temperature sensors, four control heating elements, and one perturbation heating element is used. The objective is to minimize the displacements of the structure between two fixed points due to the perturbation. The thermomechanical transfer functions between the change in heat flux at one FE surface and the change in displacement at another node by measuring the temperature change from a steady state have already been validated [3]. A Kalman filter processes these temperature

✉ F. Möller
florian.moeller@unibw.de

[1] Institute of Space Technology and Space Applications, Universität der Bundeswehr München, Werner-Heisenberg-Weg 39, 85577 Neubiberg, Germany

Published online: 15 July 2023

measurements to pass an optimal estimate to the LQR. This calculates the necessary heat fluxes for the control heating elements based on the thermomechanical structure model, so that the displacements at the desired positions in the x- and y-directions are minimized. The verification is performed by a camera system as an external validation tool, which is able to detect displacements of the structure in micrometer range. So far, it has been shown that the closed-loop filter and controller approach provides an improvement of about 4 dB compared to the uncontrolled state for a predefined, sinusoidally oscillating perturbation heat flux. In the following, the experimental setup has been revised in terms of sensor and heating element positioning and the model with filter and controller approach is able to respond to random fluctuations in the perturbation heat flux and further reduce the displacements at the target positions. The random fluctuations of the perturbation heat flux are achieved by superimposing five sinusoidal oscillations with random phase, amplitude, and frequency. In addition, a stepped change in the perturbation heating power is introduced and the system response is investigated. This allows the simulated perturbation to be compared with an actual perturbation generated on a satellite by changes in thermal boundary conditions. It is shown that, on the one hand, this method has the potential to further improve the displacement stability of already passively stabilized structures around a steady state. On the other hand, lighter and cheaper materials with poorer passive stability values could thus be made usable with the help of active structural stabilization.

In the following, the system of equations of the closed-loop filter and controller approach is briefly described first in Sect. 2. This is followed by a detailed description of the experimental setup and the experimental method. In Sect. 4, the results of the measurements are evaluated and analyzed.

2 Background

The detailed derivations for the closed filter and controller approach can be found in [1] and [3]. In the following, only a short sketch of the mathematical background will be given.

2.1 Thermomechanical FEM model

Figure 1 illustrates the FEM model of an aluminum alloy plate consisting of 100 hexahedra with 252 nodes represented by blue dots. The material data of the aluminum alloy are shown in Table 1.

The basic idea of the model includes the modal transformation of the thermomechanical problem into the frequency domain, in which transfer functions between temperature change and displacement change or between heat change and temperature change can be derived. The operability of

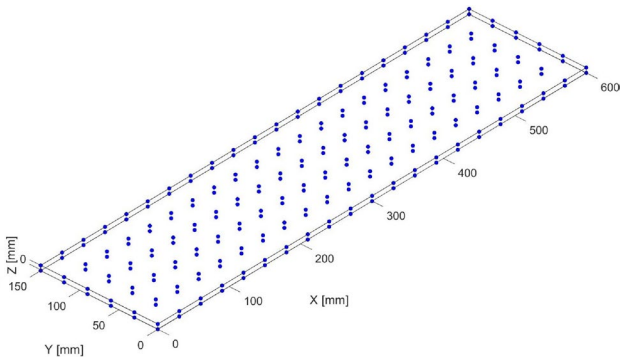

Fig. 1 FEM model of the aluminum plate

this model description has been validated in [3]. Via the state feedback of an LQR, the displacement change due to the temperature change is determined. To be able to calculate the temperature changes, temperature sensors are used, whose measurements are processed by a Kalman filter. The modal transformation allows to reconstruct the temperature field of the whole structure from the measurements of a few temperatures.

2.2 Closed-loop system

The closed-loop filter and controller approach can be described by Eq. 1

$$\begin{aligned}\left\{\delta T\right\}^{t+\Delta t} &= [A_{kal}]^{-1}[B_{kal}]\left\{\delta T\right\}^{t} + \\ &[A_{kal}]^{-1}[C_{kal}]\{\delta T_{sensor}\}_{s}^{t+\Delta t},\end{aligned} \tag{1}$$

where the matrices $[A_{kal}]$, $[B_{kal}]$, and $[C_{kal}]$ are time-invariant and, hence, can be preprocessed for a specific setup with specific system parameters, which are described in more detail in Sect. 2.3. For each new measurement at time $t + \Delta t$, Eq. 1 can be solved to determine a new temperature vector based on the previous temperature vector. Equation 2 can then be used to directly determine the necessary control heating power $\{\delta q_c\}$ for this new time step

$$\{\delta q_c\}^{t+\Delta t} = -[K_{LQR}]\{\delta T\}^{t+\Delta t} \tag{2}$$

using the gain factor matrix $[K_{LQR}]$ in the state feedback of the LQR.

2.3 System parameters

The steady state, essential for the controller, is achieved by actuating all control heating elements with a power of 0.5 W and the perturbation heating element with a power of 1 W. Based on the results from [3], different standard deviations are tested with respect to the revised experimental setup. The

Table 1 Material data EN-AW-7075 [4]

λ	c_p	ρ	E	ν	α	ϵ
130 W m^{-1} K^{-1} to 160 W m^{-1} K^{-1}	862 J kg^{-1} K^{-1}	2800 kg m^{-3}	71 GPa	0.33	23.4 K^{-1}	0.098

Table 2 Random perturbation parameters

$[\mathcal{S}_i]$	Amplitude $[\hat{y}]$	Phase $[\phi]$	Frequency $[f]$
$\mathcal{S}_1$	0.3014	3.6350	− 3.1081
$\mathcal{S}_2$	0.7112	1.4909	− 4.4040
$\mathcal{S}_3$	0.2217	2.8830	− 3.7987
$\mathcal{S}_4$	0.1761	6.0513	− 4.9848
$\mathcal{S}_5$	0.8934	3.4357	− 5.2704

standard deviations of the sensors and actuators influence the behavior of the Kalman filter and give more weight to the measurement or the estimation. For this purpose, the standard deviations for the heating elements $\sigma_H = 0.02$ W and $\sigma_H = 0.03$ W and for the temperature sensors $\sigma_T = 0.075$ K, $\sigma_T = 0.10$ K and $\sigma_T = 0.12$ K have been implemented in the Kalman filter. According to the manufacturer, the latter are between 0.1 K and 0.2 K [5]. However, by calibration (refer to Sect. 3.2), these can be reduced with respect to the simulation, so that the Kalman filter can give a higher weighting to the sensor measurements. In this work, the response of the system to a sinusoidal perturbation as well as to a random perturbation is tested. The sinusoidal perturbation is identical to [3] with an amplitude of 0.5 W and a period of 6 h, corresponding to a frequency of 4.63×10^{-5} Hz, thus satisfying the requirements of low-frequency changes due to the thermal problem. The randomly generated perturbation is achieved by a superposition of five sinusoidal oscillations with phases, amplitudes, and frequencies listed in Table 2. Each individual sinusoidal perturbation $\mathcal{S}_i(t)$ is given by Eq. 3 as

$$\mathcal{S}_i(t) = \hat{y}_i \sin(2\pi \cdot 10^{f_i} \cdot t + \phi_i). \tag{3}$$

The values for amplitude, frequency, and phase were generated using the MATLAB built-in function *rand*, which outputs uniformly distributed (pseudo) random numbers within a defined interval. The value ranges for amplitude, frequency, and phase were defined to be [0, 1],[-3, -6], and $[0, 2\pi]$, respectively. Subsequently, the values were saved, so that the same random perturbation can be used for each test, ensuring the reproducibility of the results. Figure 2 shows the variation of the randomly generated perturbation around the steady state of 1 W for a duration of 48 h. Nevertheless, a duration of only 24 h was mostly used for the tests, as this is sufficient to be able to show the functionality.

The application of stepped changes in the heating power is intended to simulate the switching on and off of electrical devices that do not continuously dissipate energy. For this purpose, eight steps were defined for a test with a running time of 24 h. The exact parameters can be taken from Table 3. Figure 3 shows the course of the change of the disturbance heating power from the steady state of 1 W.

3 Experimental setup

Figure 4 shows the schematic experimental setup. Temperature sensors and heating elements are mounted on the surface of the aluminum plate, which in turn is mounted on an isostatic support in the Thermal Vacuum Chamber (TVC). To simulate the radiation background of space, temperatures on all inner surfaces of the TVC are stabilized by a Process

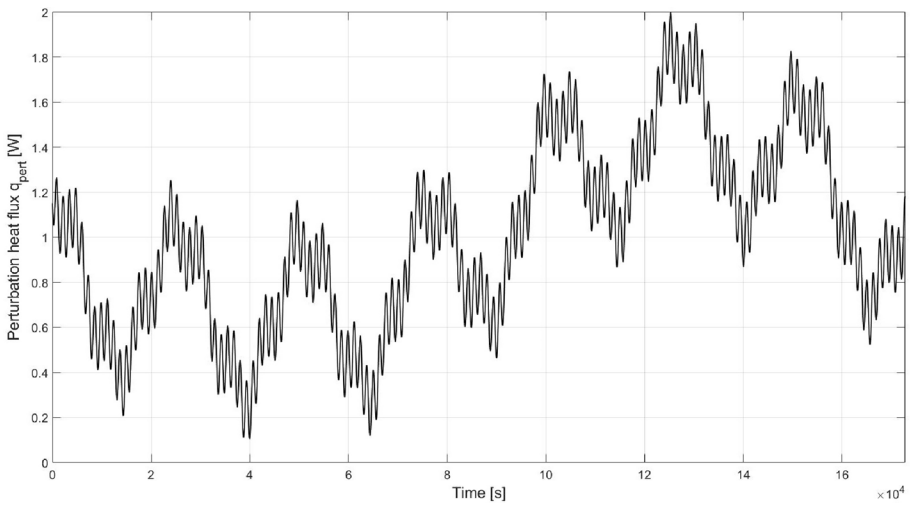

Fig. 2 Random perturbation

Table 3 Stepped perturbation parameters

Step	Amplitude	Duration
1	+0.75 W	6 h
2	+0.25 W	6 h
3	0 W	1 h
4	− 0.25 W	1 h
5	0 W	1 h
6	+0.75 W	1 h
7	0 W	1 h
8	+0.25 W	1 h

Cooling Unit (PCU). Outside the TVC, the temperature measurements recorded by the data acquisition system are processed and the required control power for the heating elements is calculated. To measure the distortions of the plate, a speckle pattern is applied to the surface of the test object. Using a high-resolution camera and a Digital Image Correlation (DIC) software, the change in gray levels of the speckle pattern is captured and the pixels of the camera images are precisely assigned to the local surface pattern [6, 7]. Images acquired at 10-min intervals are then analyzed using subpixel-accurate image correlation algorithms. LEDs are positioned inside the TVC to illuminate the object, which are activated in time synchronization with the image acquisitions. This prevents the radiation influence of the LEDs from affecting the temperature equilibrium.

Figures 5 and 6 show the front and rear views of the experimental setup. The front is covered with a speckle

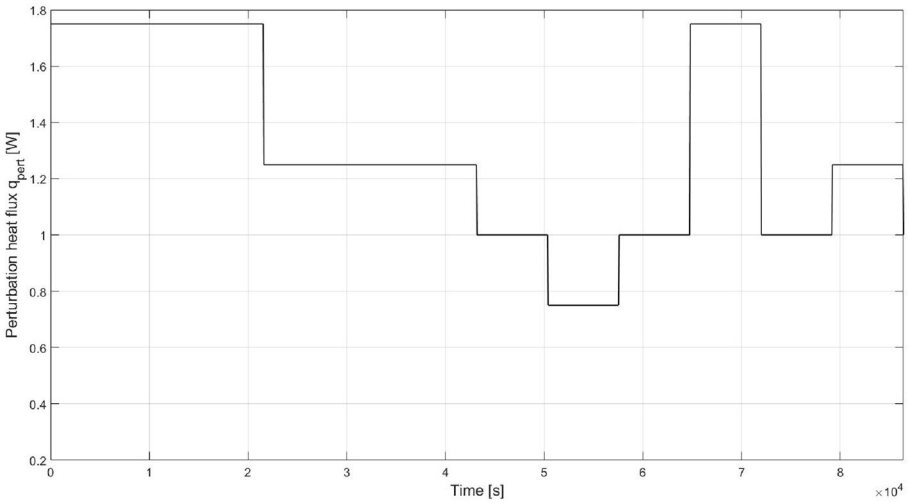

Fig. 3 Stepped perturbation

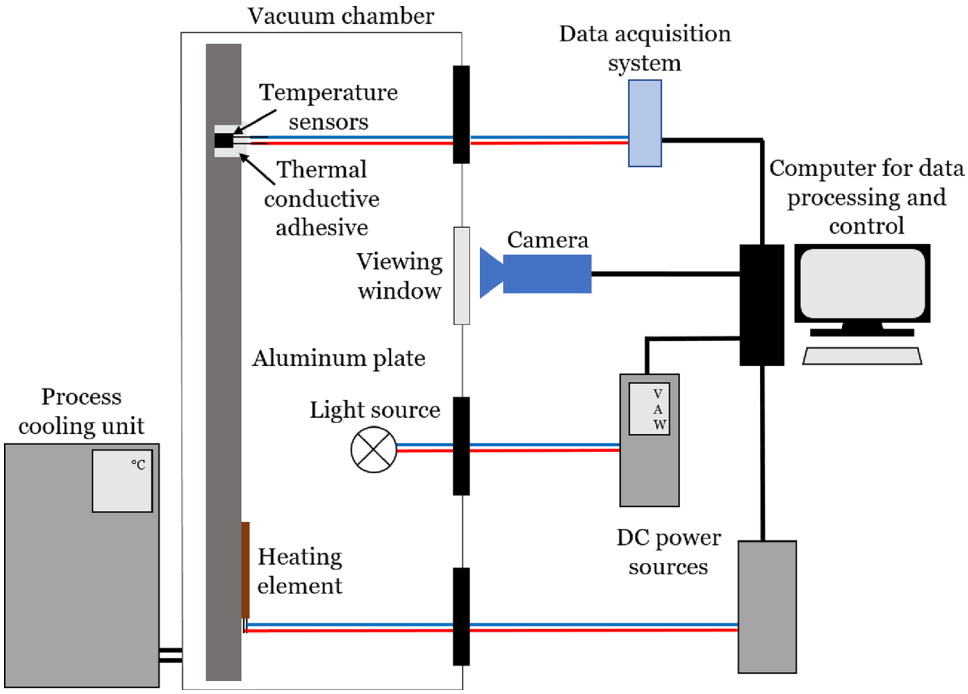

Fig. 4 Schematic experimental setup

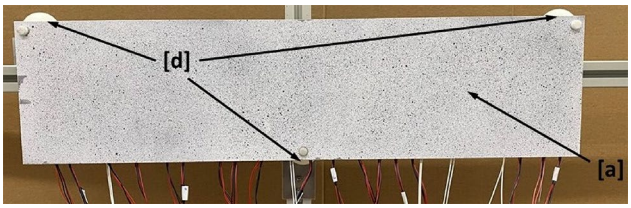

Fig. 5 Experimental setup, front view

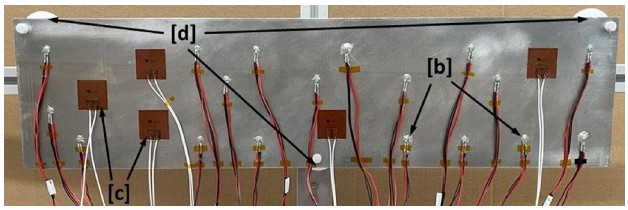

Fig. 6 Experimental setup, rear view

pattern ([a] in Fig. 5), so that the displacements can be measured by the DIC camera. Sensors ([b] in Fig. 6) and heating elements ([c] in Fig. 6) are mounted on the back. The isostatic mount in the 3–2–1 configuration ([d] in Fig. 5 and 6) allows free expansion of the structure by blocking only 6 degrees of freedom [8]. The balls in the brackets made of Polytetrafluorethylen (PTFE), whose thermal conductivity is 520 times lower than that of aluminum [4, 9], serve to thermally decouple the structure [10] from the frame to which the aluminum plate is attached.

PT-100 temperature sensors with an accuracy of up to 0.1 K are used for temperature measurement [5]. They are attached with a silver-based, vacuum-compatible, highly thermally conductive adhesive. This allows the plate and sensor to bond with virtually no change in emissivity, enabling temperature measurement in vacuum [11]. A USB data acquisition system is used to convert resistance measurements into temperature measurements via a shunt resistor. The line and connection resistances caused by wiring and connectors are thus negligible [12]. The sensor readings acquired and stored with Data Acquisition System Laboratory (DASYLab) [13] are then processed using an MATLAB program. By setting various steady-state temperature conditions with the PCU and making appropriate comparison measurements, the temperature sensors mounted on the plate can be calibrated. Self-adhesive vacuum-compatible Kapton heating foils are used as heating elements [14]. They are operated with DC power sources, which in turn are commanded via an MATLAB interface and thus serve as control elements. Since the resistance of the heating elements is known without wiring and connections, the necessary current for a desired heating power can be calculated. Due to the stationary temperature control of the test setup by the PCU, thermally induced losses via plug and cable connections can be neglected. The efficiency of a heating element is thus close to 100 %.

3.1 Revision of the setup

One of the objectives of this paper is to revise the experimental setup used in [3] with respect to the positioning of sensors and heating elements to reduce the displacements and necessary control heating power.

In a first step, the positions of the control heating elements are revised for this purpose. The two nodes to be controlled in x- and y-directions are highlighted in red in Fig. 7 and marked with the numbers 1 and 2. One heating element must be used for each degree of freedom. Each of these can only be placed on one side of the plate, since the other side is covered with the speckle pattern for the camera images. The artificial perturbation in the form of a perturbation heating element, marked in red in Fig. 7, is also predefined. In the simulation of the closed-loop filter and controller approach, brut force [15] is now used to systematically try every possible position for each of the four control heating elements, while the controller result is evaluated for the optimal positions of the temperature sensors in each case. The optimal

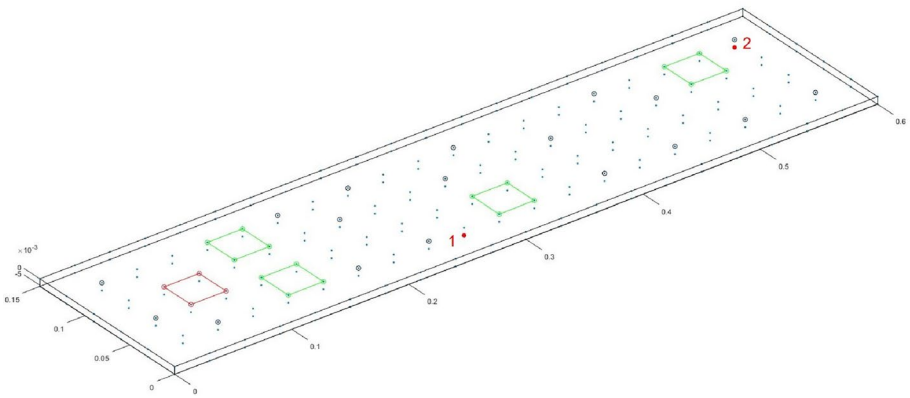

Fig. 7 Revised configuration of the test setup

positions of the temperature sensors in turn are obtained by ranking the largest modal weights of each node. Additional criteria are defined to reduce the computational cost. Heating elements should not be placed directly next to each other due to the wiring, nor should they be placed on or in close proximity to the isostatic mounts. For closer consideration, those distributions of the control heating elements are then selected for which control of the two nodes with the lowest possible heating power δq_c and an improvement of the displacements by at least a factor of 4 compared to the uncontrolled condition is possible in the presence of sinusoidal perturbation. Subsequently, an exclusion of those cases that do not achieve the required improvement of the displacement for a random perturbation is performed. In a final step, the sensor positions from the remaining cases are adapted for a technical realization. The sensors can also be placed only on one side of the plate, and neither on the edge nor directly on the heating elements. Also, an accumulation of many sensors in one area of the plate must be avoided for a better reconstruction of the temperature field. The resulting configuration is shown in Fig. 7.

3.2 Calibration of the test setup

Calibration of the sensors and actuators forms the basis of successful validation of the system. To be able to guarantee the required power at the heating elements correctly at all times, no classical calibration is necessary. Since the resistance of the heating elements is specified by the manufacturer with 14 Ω [14] and has been confirmed by tests, the resistance of the wiring and feed-through can be regarded as connected in series, taking into account Ohm's law, and thus, the necessary current for a desired heating power can be calculated directly.

A perfect representation of the reality is not possible on both sides, the FEM model, as well as the experimental setup. The combination of model and experimental setup causes errors, especially in the interfaces with sensors and actuators. From the thermomechanical model, simplifications are made in favor of the performance. These include the neglect of the mechanical short-term dynamics and the influences of the weight force on the plate. In addition, the plate is modeled to be in free space. Thus, thermal influences of the isostatic support and the experimental setup are ignored. Experimental validation of the transfer functions [3] has confirmed that these influences are negligible. The accuracy of the FEM model is further limited by the size of the actuators (heating elements), since the minimum size of a surface element in the FE model must be equal to the size of a heating element. Thus, the description of the system remains coarse, but still valid and performant.

On the side of the experimental setup, an optimal placement of the heating elements and temperature sensors cannot be guaranteed. Losses occur due to bonding, cabling, and radiation as well as inhomogeneous heat input due to the nature of the heating elements. There is potential for optimization in this area, particularly with regard to temperature data acquisition. In an extension of the calibration of the sensors for stationary, homogeneous temperature fields [16], the differences between the model side and the experimental side for stationary, inhomogeneous temperature fields are investigated in this work.

Figure 8 shows for different steady-state, inhomogeneous conditions, which differ mainly by the applied heating power, a linear dependence between applied total heating power $\bar{P}_{plate}$ and the average measured temperature. Figure 9 shows the temperature deviations $\delta\bar{T}_{plate}$ between simulation and measurement of one individual sensor i (here Sensor 8, exemplary) for those different steady-state conditions with different simulated emissivities of the speckle pattern. The deviations are in a range of $\pm$ 0.4 K and are thus larger than the standard deviation of the sensors, which is why they must be compensated. This systematic deviation can be attributed to errors of the model as well as those of the experimental setup, as described before. Since a model-side correction is much more complex compared to a correction of the measured values and the fitting of the sensor data allows a more powerful integration into the Kalman filter, a dynamic correction function for the measured values was derived, which is expressed by Eqs. 4 and 5

$$\bar{P}_{plate} = a \cdot \bar{T}_{plate} + b \tag{4}$$

$$\delta T_i = c_i \cdot \bar{P}_{plate} + d_i. \tag{5}$$

Here, a and b stand for the linear factors of the function from Fig. 8 and c_i and d_i for the linear factors for a sensor i from Fig. 9. The linear factors are determined from the measured values using the least squares method [17]. Combining both correlations, the measured average temperature of the plate $\bar{T}_{plate}$ can be used to approximate the total applied heating power $\bar{P}_{plate}$, and by substituting into Eq. 5 calculate a temperature value correction δT_i for each sensor i. Considering the discrete temperature measurement with low controller and system dynamics, the measurement states are considered to be quasi-stationary. This should allow an inference of the plate temperature averages, based on the correlation 4 determined for stationary, inhomogeneous states. The goal is to improve sensor accuracy relative to simulation. The implications of the procedure are discussed in Sect. 4.

4 Results and validation

The results obtained by [3] are used as a basis for the emissivity analysis of the setup and the validity of the transfer functions. Based on this, the results of the revised

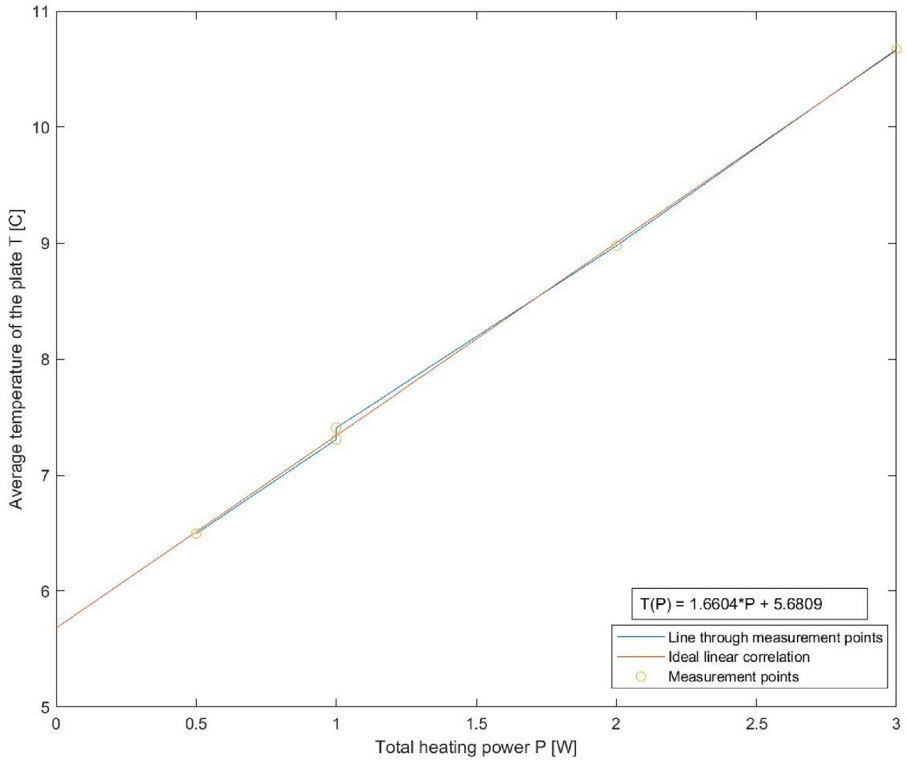

Fig. 8 Correlation between average temperature and heating power

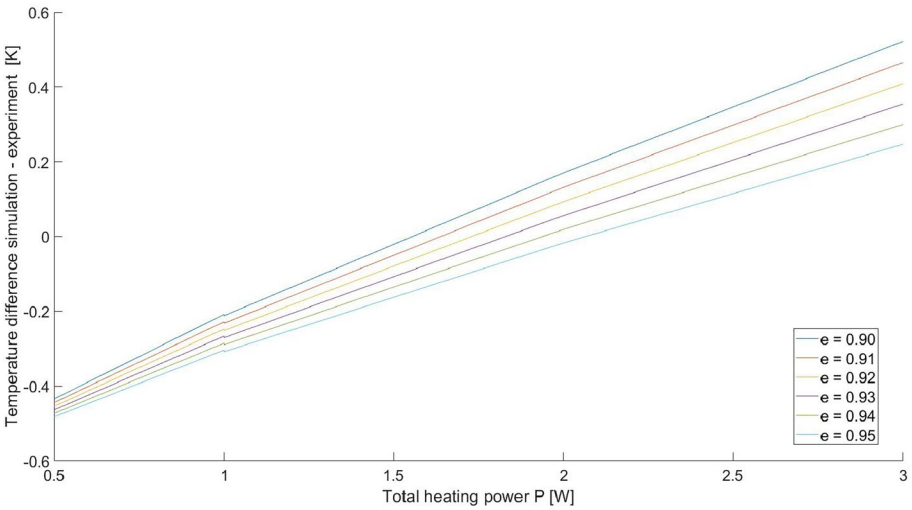

Fig. 9 Correlation between temperature deviation of sensor 8 and heating power

experimental setup for a sinusoidal perturbation are compared with those of the initial experimental setup. Finally, the ability of the system to respond to a random perturbation is shown.

The displacements presented in the following sections are based on the distances between the control points defined in Sect. 3.1. The camera system determines the displacements in x- and y-directions from the correlation of these points, as well as the total displacement as vectorial addition. The coordinate system for the evaluation is chosen in such a way that the origin lies on the point inert in all three translational directions of motion (right, upper mount in Fig. 5). The x-axis is parallel at the outer edge of the plate toward the center and the y-axis is upward away from the plate. Thus, a positive x-value describes an expansion in the direction of the plate length and a negative y-value describes an expansion in the direction of the plate width.

4.1 Emissivity analysis

Since a change in the emissivity of the plate is possible by sealing the speckle pattern, an analysis is performed based

on the steady-state inhomogeneous measurements from Sect. 3.2. The sealing of the speckle pattern for a vacuum application is realized by applying a PTFE-slide coating. The emissivity of the plate without this sealing is given as $\epsilon = 0.93$ in [3]. Since PTFE is assigned a value of 0.92 in the literature [18], the range of values for the analysis is limited to 0.90 to 0.95. After correcting the temperatures by the procedure described in Sect. 3.2, the simulated emissivity is chosen which has the lowest mean deviation of all sensors from the real measurement. The value here also results in $\epsilon = 0.93$.

4.2 Sinusoidal perturbation

In this section, the responses of the system to a sinusoidal perturbation are compared with those of [3].

4.2.1 Uncontrolled system

Figure 10 shows the displacements of the uncontrolled system visualized by the camera system. In addition, the course of the sinusoidal perturbation is shown in black. As a complement, Fig. 11 shows the temperature course of all 18 sensors for the sinusoidal perturbation. Both figures clearly reflect the sinusoidal perturbation and a phase shift of the maxima between perturbation and displacement of about 40 min can be seen, as expected from the simulation.

In comparison with the results from [3], two phenomena appearing unusual also show up. First, a linear displacement of the symmetry axis can be seen around which the sinusoidal displacements oscillate. As a consequence, it can be concluded that the system cannot reproduce the reversibility of the thermal displacements. On the one hand, this may be due to the non-ideal, isostatic mount and, on the other hand, to measurement inaccuracies in the camera system. It must be noted that measurement ranges of a few µm place significant demands on sensors and overall setup. In addition, the dynamics of the perturbation override the inherent dynamics of the material, so that a new maximum in the perturbation occurs before the material could return to its initial state. Second, the measured values of the displacements order around the

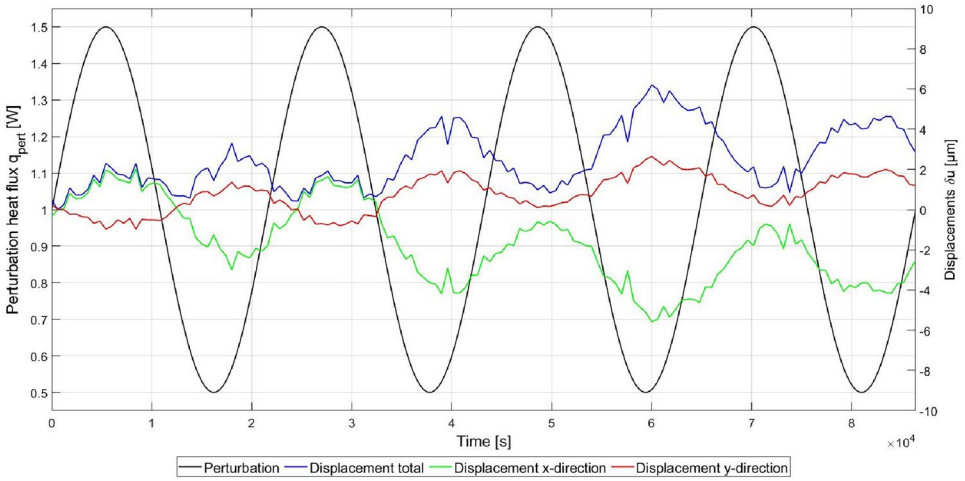

Fig. 10 Displacement, uncontrolled

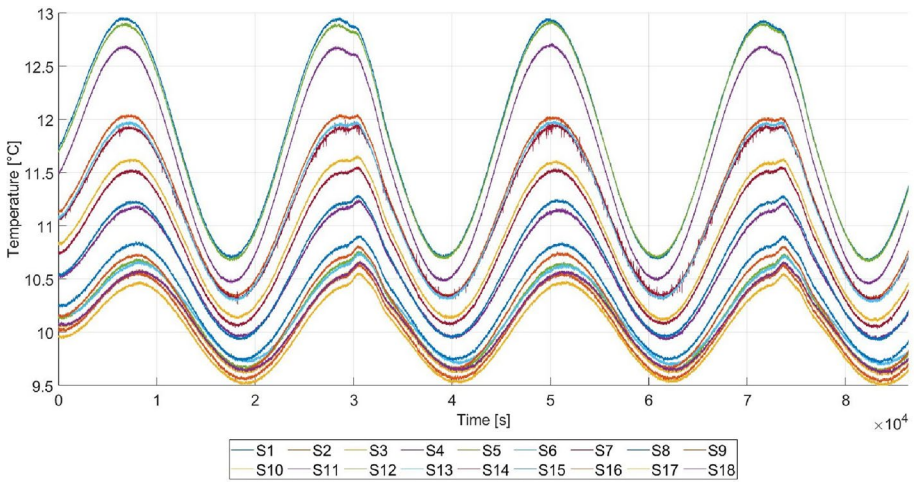

Fig. 11 Temperature curve, uncontrolled

expected value of 7 µm, resulting from the initial length between the control points of 0.3 m and a temperature amplitude of approximately 1 K. Here, inaccuracies in the experimental setup, as well as perturbations of the camera system measurements, will have an influence. The fact that the displacements determined in this work are below the expected value, in contrast to the comparative values from [3], may be related to the reduction of the power of the control elements in steady state from 0.6 W to 0.5 W. The representation of the processes was judged to be sufficient for an investigation of the principle of operation. In addition, Fig. 10 clearly shows that the displacements in the x-direction have a significantly larger amplitude than those in the y-direction. This is due to the geometry of the test object. To capture images using the DIC system, the camera needs to be positioned outside of the TVC in front of a circular viewport. The maximum size of an object that can be captured is achieved when the camera is positioned in the center of the viewport. The longest distance in a spatial direction is thus achieved by a rectangular object. To demonstrate the capability of the approach to sufficiently compensate for displacements in both the x- and y-directions, a square test object would be more suitable. However, using a square shape would also reduce the distance between the points to be stabilized, resulting in a decrease in the amplitude of the measured displacement, which would be less distinguishable from the resolution of the camera system. Therefore, the rectangular shape was also used for the revised test setup.

4.2.2 Comparison of the controlled systems

For the standard deviations of the temperature sensors σ_T the values $\sigma_T = 0.10\,\mathrm{K}$ and $\sigma_T = 0.12\,\mathrm{K}$ can be compared with those from [3]. The value for the standard deviation of the heating elements $\sigma_H = 0.02$ remains identical. Tables 4 and 5 compare the values of the former and the revised setup. Those values represent the respective maximum mean displacements in a given spatial direction and are extended by a factor relative to the displacement of the uncontrolled system. In addition, the maximum commanded control heating powers $Q_{c,max}$ of the filter-controller approach are plotted in the last row. In comparison, the absolute displacements of the revised experimental setup appear to be lower, which can be explained by the lower heating power used for the steady-state condition of the control heating elements.The reductions of the displacements are not stronger in the improved experimental setup, for $\sigma_T = 0.10\,\mathrm{K}$, even a deterioration seems to occur compared to the previous experimental setup. However, it can be seen that for a similar degree of structural stabilization, much less control heating power $Q_{c,max}$ is required, and thus, the system is more efficient.

Table 4 Displacements and control performance for [3]

Direction	Uncontrolled	$\sigma_T = 0.10\,\mathrm{K}$ (Factor)	$\sigma_T = 0.12\,\mathrm{K}$ (Factor)
Total	8.93 µm	4.39 µm (2.03)	3.11 µm (2.87)
x	10.10 µm	6.33 µm (1.60)	5.24 µm (1.93)
y	4.77 µm	3.15 µm (1.51)	2.54 µm (1.88)
$Q_{c,max}$	–	1.09 W	0.95 W

Table 5 Displacements and control performance, revised

Direction	Uncontrolled	$\sigma_T = 0.10\,\mathrm{K}$ (Factor)	$\sigma_T = 0.12\,\mathrm{K}$ (Factor)
Total	6.20 µm	3.97 µm (1.56)	2.49 µm (2.49)
x	5.58 µm	3.56 µm (1.57)	2.16 µm (2.58)
y	2.64 µm	1.83 µm (1.44)	1.19 µm (2.22)
$Q_{c,max}$	–	0.7 W	0.66 W

4.2.3 System parameters $\sigma_T = 0.075\,\mathrm{K}, \sigma_H = 0.03\,\mathrm{W}$

As a fit to the corrected temperature sensor measurements, an experiment was performed with a lower standard deviation for the temperature sensors of $\sigma_T = 0.075\,\mathrm{K}$, but a higher standard deviation for the heaters of $\sigma_H = 0.03\,\mathrm{W}$ for a sinusoidal perturbation. Figures 12 and 13 show the commanded control heating powers and the temperature response of all sensors for the controlled structure.

The amplitudes of the temperature response are only seen in those sensors closest to the perturbation and, with values of 0.25 K, are much lower than those of the uncontrolled structure from Fig. 11. However, the maximum commanded control heating powers, $Q_c = 0.76\,\mathrm{W}$, are between the values of Tables 4 and 5.

Figure 12 shows, representative for all Q_c-courses of the revised experimental setup, that primarily control heating elements 1 and 2 compensate the perturbation. The reason for this is the positioning of those heating elements on the symmetry axis of the plate. Due to a fault in the temperature control, the PCU is not able to keep the ambient temperature constant at 5 °C. Instead, the controller performs an activity roughly every 12 h, which is reflected in the curves of temperature and control heating powers. It can be seen very clearly in Fig. 12 that the control heaters 3 and 4 compensate for the perturbations to the system caused by the PCU.

Looking at the displacements in Fig. 14, it can be seen that the course can be divided into two parts. Up to a time of 3.5×10^4 s, the values remain stable in a certain range. Then, a transition occurs up to 4.7×10^4 s, after which the values remain stable again. This displacement of the baseline, or steady state, around which the displacements fluctuate can be attributed to the significant temperature

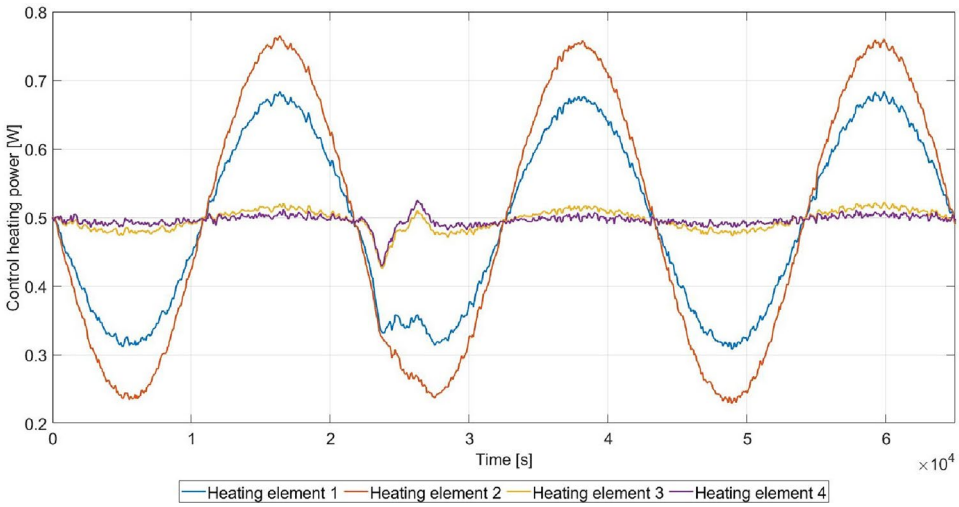

Fig. 12 Control heating power, $\sigma_T = 0.075$ K

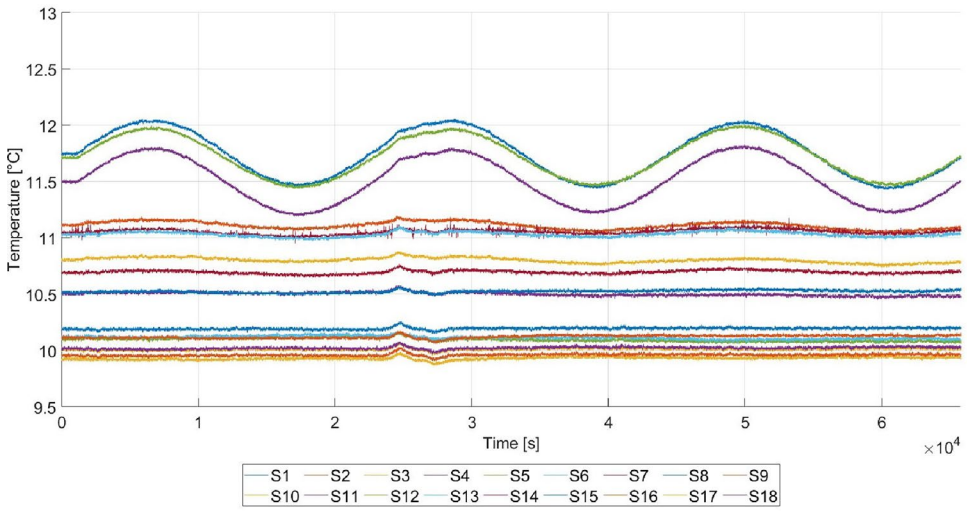

Fig. 13 Temperature curve, $\sigma_T = 0.075$ K

variations between day and night. The camera system is exposed to these within the laboratory. A key indication of this is that there is no temperature variation manifested in Fig. 13 for this transition, and thus no basis for thermal displacement within the system. For stabilization in the time range from 0 s to 3.5×10^4 s, factors well above 2 can be determined, which yield better results compared to the other tests. An overview of the values can be found in Table 6. These refer to the first part.

4.3 Random perturbation

In the following section, the responses of the system to a random perturbation are shown according to the parameters defined in Sect. 2.3. The analysis is based on a time interval of 24 h.

4.3.1 Uncontrolled system

Figure 15 shows the course of the random perturbation in black as well as the resulting average total displacements with the contributions in x- and y-directions. Significant total displacements are shown with a dominant component in the x-direction. Quantitatively, the displacements are significantly larger than those of the sinusoidal perturbation from section 4.2.1, which is due to the stronger fluctuations in the perturbation heating power Q_{pert}. The maximum total displacement is 10.36 µm.

Figure 16 shows the temperature profile of the individual sensors in the uncontrolled case for the random perturbation. The temperatures fluctuate by about 2 K at the maximum. However, the high-frequency components of the thermal perturbation can be seen only in the temperature sensors in the immediate surroundings of the perturbation heating

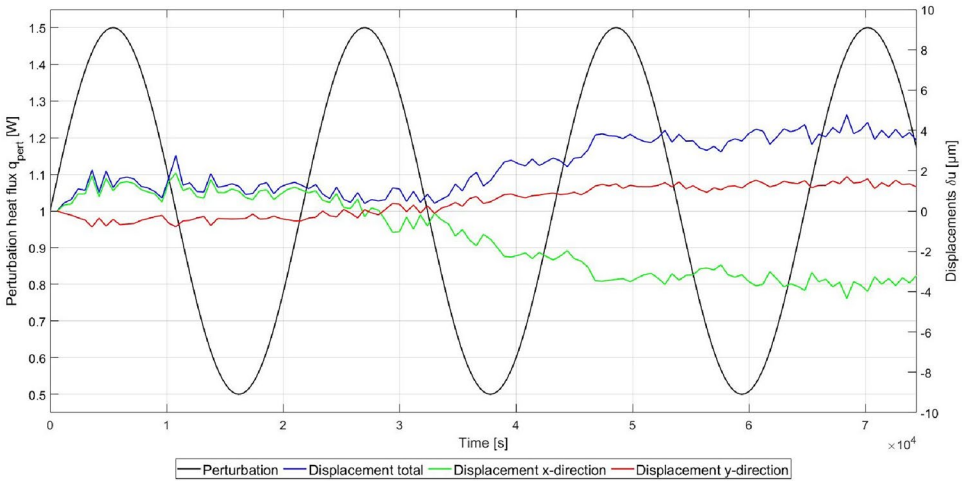

Fig. 14 Displacement, $\sigma_T = 0.075$ K

Table 6 Displacement, sin. pert., $\sigma_T = 0.075$ K

Direction	Uncontrolled	Controlled	Difference	Factor
Total	6.20 µm	2.76 µm	3.44 µm	2.25
x	5.58 µm	1.88 µm	3.70 µm	2.97
y	2.64 µm	0.79 µm	1.85 µm	3.34

element. At the beginning of the chart, there is a period of approximately 90 min where the temperature fluctuations of each sensor are below 0.01 ∘C. This defines the steady state, which is used as a reference for each individual experiment. In the subsequent temperature diagrams, the display of this steady state is omitted in favor of time synchronization with the displacements and heating power.

4.3.2 System parameters $\sigma_T = 0.10$ K, $\sigma_H = 0.02$ W

Figures 17 and 18 show the commanded control heating powers and temperature response of all sensors for the controlled structure with $\sigma_T = 0.10$ K in response to the random perturbation. Due to an error in the PCU, only data over a time range of 13 h are available for this experiment. In Fig. 17, it can also be seen that, primarily, the control heating elements 1 and 2 are triggered by the filter-controller system. The high-frequency components of the perturbation in the course of Q_c can also be seen here. As a result of the higher perturbation heating power Q_{pert}, the maximum control heating power is with $Q_{c,max} = 0.8$ W above that of the sinusoidal perturbation. In the temperature plot in Fig. 18, maximum fluctuations of a sensor of 0.75 K can be noticed. Moreover, the temperature field is qualitatively much more stable than that of the uncontrolled system. Perturbations are strongly attenuated with increasing distance from the perturbation heating element, so that only 3 of the 18 sensors can be identified with the perturbation.

The resulting displacements are shown in Fig. 19. A high stability in all spatial directions can be observed. The course of the perturbation is also plotted, so that it can be seen that the resulting displacements do not follow this perturbation.

The exact comparison values can be taken from Table 7.

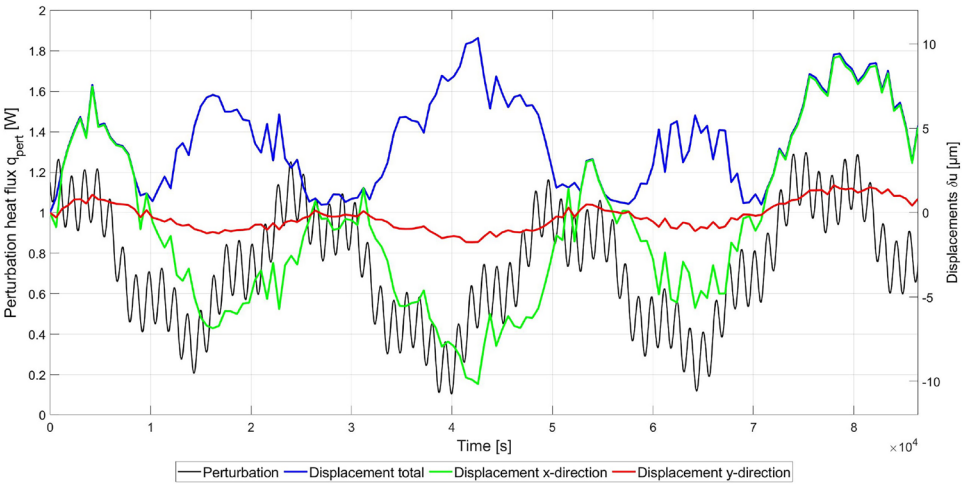

Fig. 15 Uncontrolled displacement, random pert

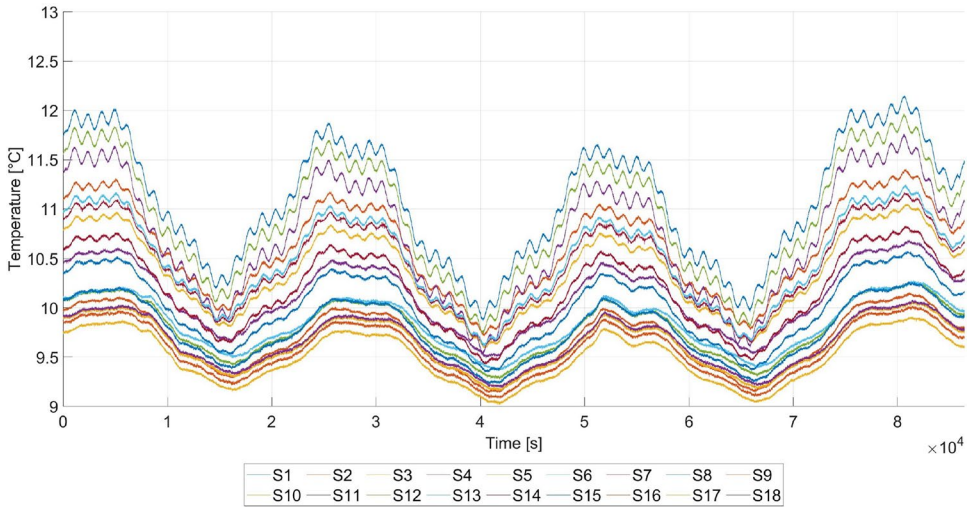

Fig. 16 Uncontrolled temperature curve, random pert

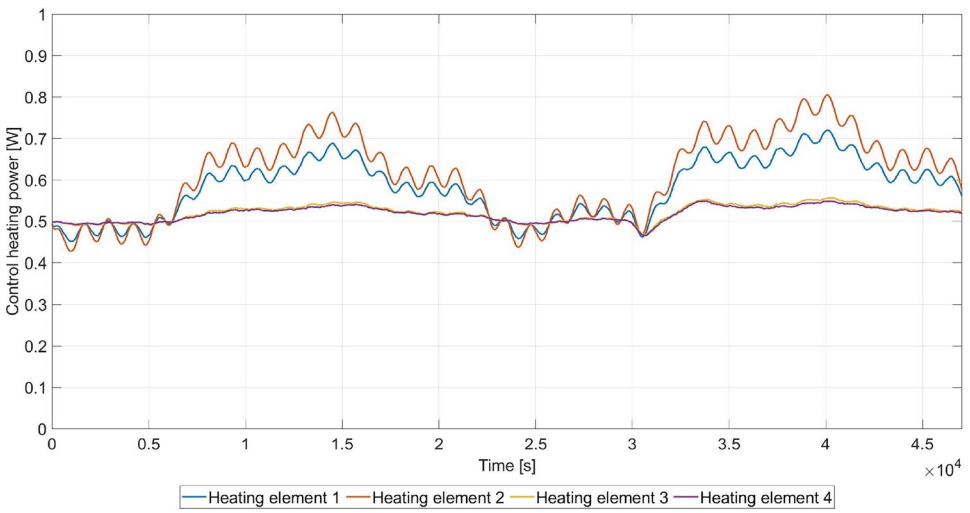

Fig. 17 Control heating power, random, $\sigma_T = 0.10\,\mathrm{K}$

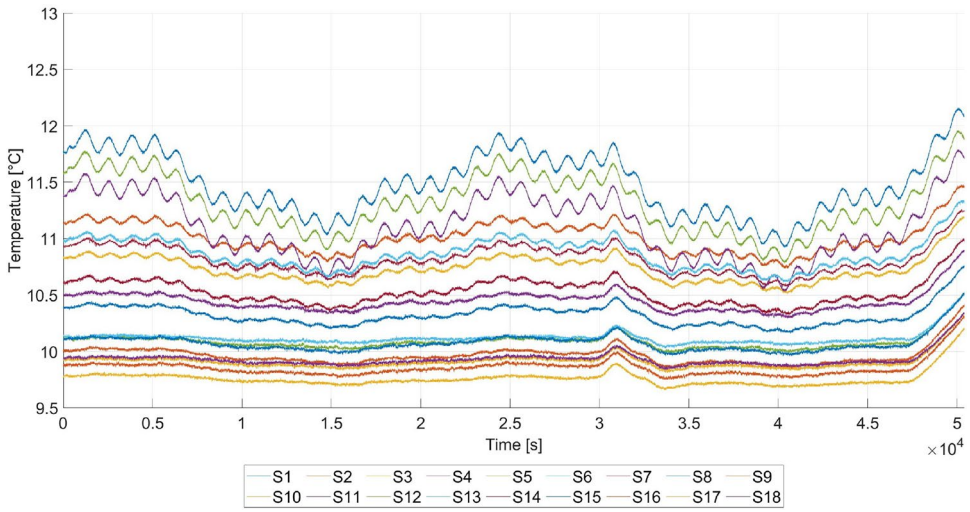

Fig. 18 Temperature curve, $\sigma_T = 0.10\,\mathrm{K}$

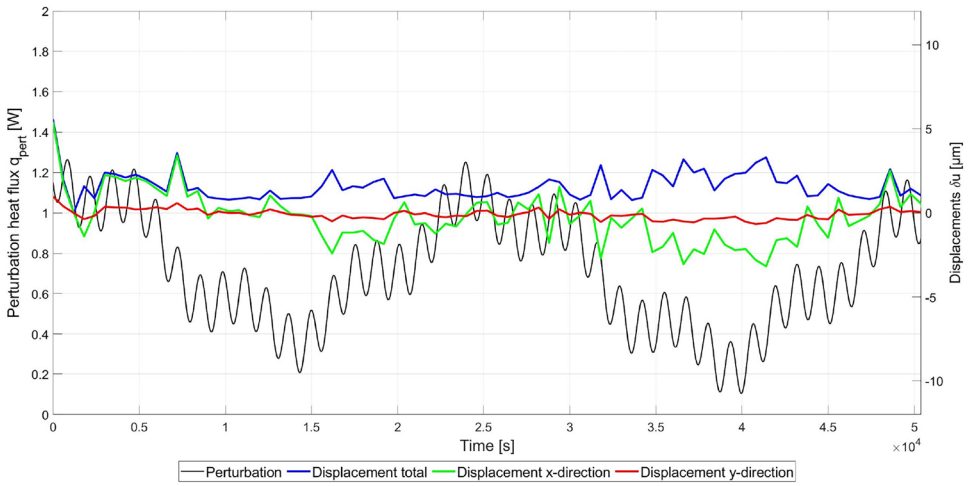

Fig. 19 Displacement, random, $\sigma_T = 0.10$

Table 7 Displacement, random, $\sigma_T = 0.10\,\mathrm{K}$

Direction	Uncontrolled	Controlled	Difference	Factor
Total	10.36 µm	3.57 µm	6.79 µm	2.90
x	10.15 µm	3.42 µm	6.73 µm	2.97
y	1.63 µm	0.66 µm	0.97 µm	2.47

4.3.3 System parameters $\sigma_T = 0.12\,\mathrm{K}$, $\sigma_H = 0.02\,\mathrm{W}$

Figures 20 and 21 show the commanded control heating powers and temperature response of all sensors for the controlled structure with $\sigma_T = 0.12\,\mathrm{K}$ in response to the random perturbation. In direct comparison to the previous test (see Sect. 4.3.2), the course of the commanded heating power Q_c is almost identical and can be attributed to the same causes. The maximum control heating power is only slightly smaller with $Q_c = 0.76\,\mathrm{W}$. The temperature profile is also qualitatively very similar.

Figure 22 shows the displacement between the two control points. A stable course can be seen up to 4.5×10^4 s. After that, the behavior described in Sect. 4.2.3 is repeated. Again, no change in the temperature field can be inferred from the temperature profile that could cause such a displacement. However, the changes in the environmental temperatures were almost on the same level for that test. Hence, the data for the intervals $t_1 \in [0\,\mathrm{s}, 4.5 \times 10^4\,\mathrm{s}]$ and $t_2 \in [0\,\mathrm{s}, 8.64 \times 10^4\,\mathrm{s}]$ are evaluated. For the interval t_2, there is no significant stabilization effect due to high fluctuations and peaks in the displacement. However, for the interval t_1, there is a good stabilization of the system with a reduction of the displacement between the control points by a factor of 3. A detailed comparison of the values to those of the uncontrolled case can be taken from Table 8.

4.3.4 System parameters $\sigma_T = 0.075\,\mathrm{K}$, $\sigma_H = 0.03\,\mathrm{W}$

Figures 23 and 24 show the commanded control heating powers and temperature response of all sensors for the

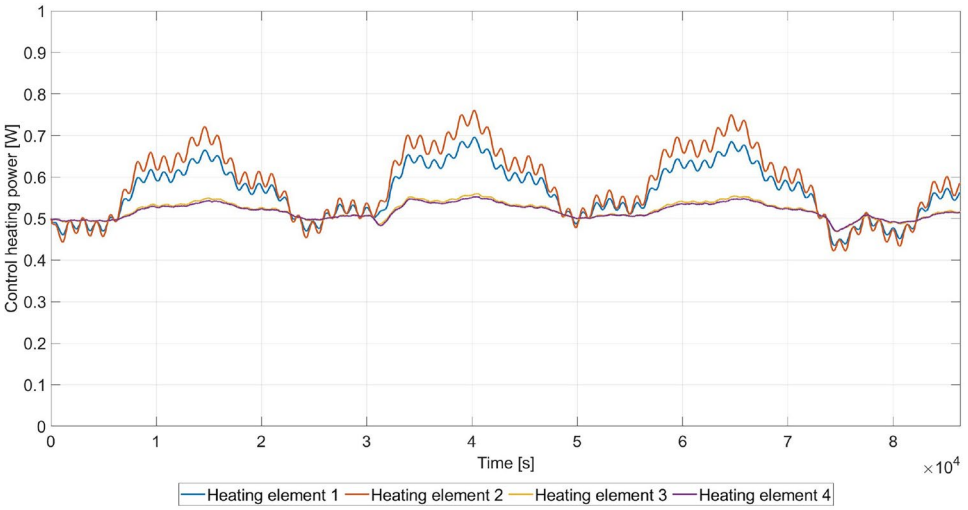

Fig. 20 Control heating power, random, $\sigma_T = 0.12\,\mathrm{K}$

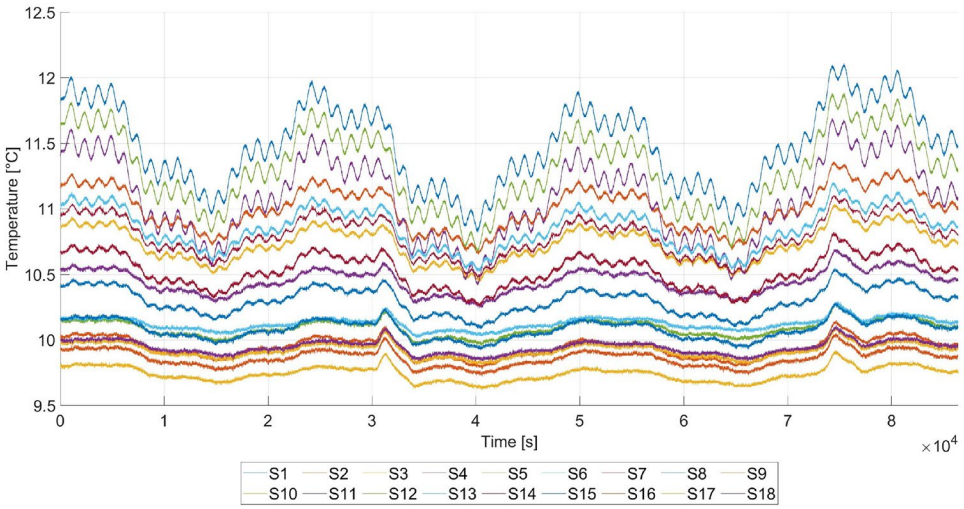

Fig. 21 Temperature curve, random, $\sigma_T = 0.12\,\mathrm{K}$

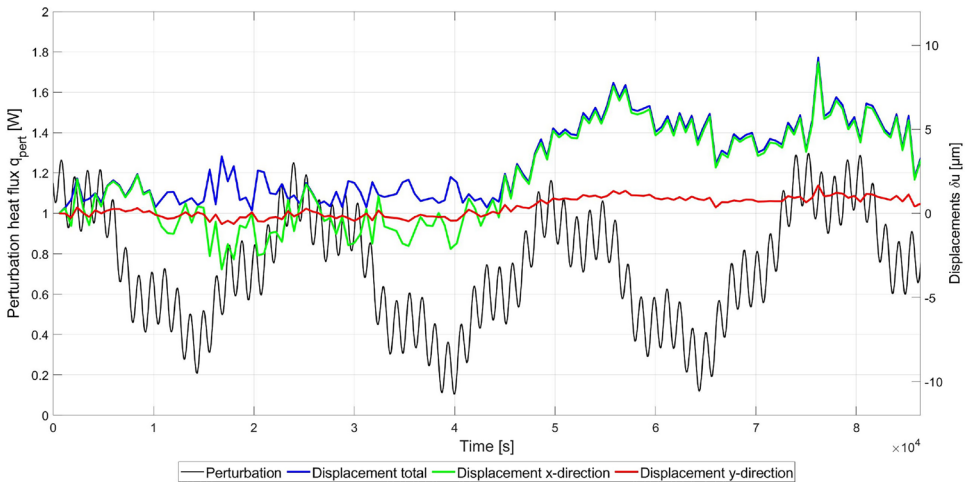

Fig. 22 Displacement, random, $\sigma_T = 0.12$

Table 8 Displacement, random, $\sigma_T = 0.12\,\mathrm{K}$

Direction	Uncontrolled	Controlled	Difference	Factor
Total	10.36 µm	3.39 µm	6.97 µm	3.06
x	10.15 µm	3.33 µm	6.82 µm	3.05
y	1.63 µm	0.63 µm	1.00 µm	2.59

controlled structure with $\sigma_T = 0.075\,\mathrm{K}$ in response to the random perturbation.

In direct comparison to the two previous tests (Sects. 4.3.2 and 4.3.3), the deflections of the commanded heating power Q_c are larger and the curves for the individual heating elements are more dynamic, so that high-frequency portions of the perturbation can also be seen in control heating elements 3 and 4. The maximum control heater power, $Q_c = 0.99\,\mathrm{W}$, exhausts the available range of values from 0.00 W to 1.00 W. A significant improvement in the stabilization of the temperature field can be seen in the temperature profile with maximum fluctuations of only 0.45 K. Consequently, Fig. 25 shows a very well-stabilized displacement curve with an improvement to the uncontrolled case by a factor of 3 in all displacement directions, provided that the region between 1.8*e*4 s and 2.7*e*4 s is excluded, which is not due to any relevant influences and thus considered as a interference of the camera system. A detailed comparison of the values to those of the uncontrolled case can be taken from Table 9.

4.4 Stepped perturbation

Figures 26 and 27 show the commanded control heating powers and temperature response of all sensors for the controlled structure with $\sigma_T = 0.1\,\mathrm{K}$ and $\sigma_H = 0.02\,\mathrm{W}$ in response to the stepped perturbation. It can be clearly seen that the changes in the control heating powers follow the step changes perturbation in opposite directions. This shows that the system seems to respond adequately to this type of perturbation, as well.

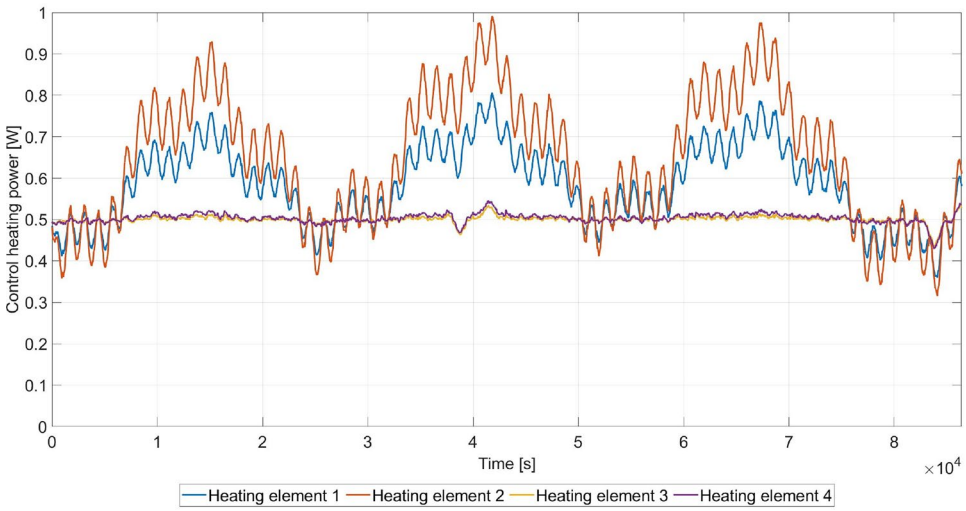

Fig. 23 Control heating power, random, $\sigma_T = 0.075$ K

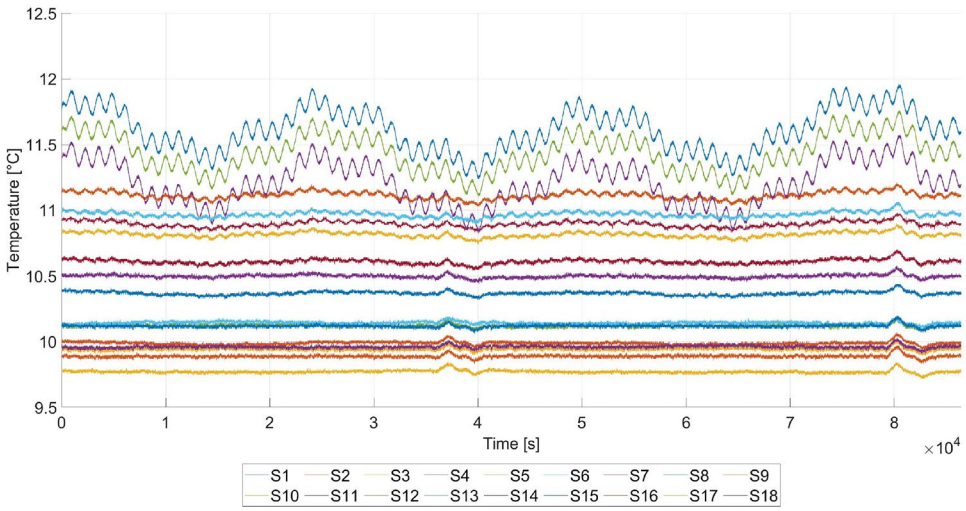

Fig. 24 Temperature curve, random, $\sigma_T = 0.075$ K

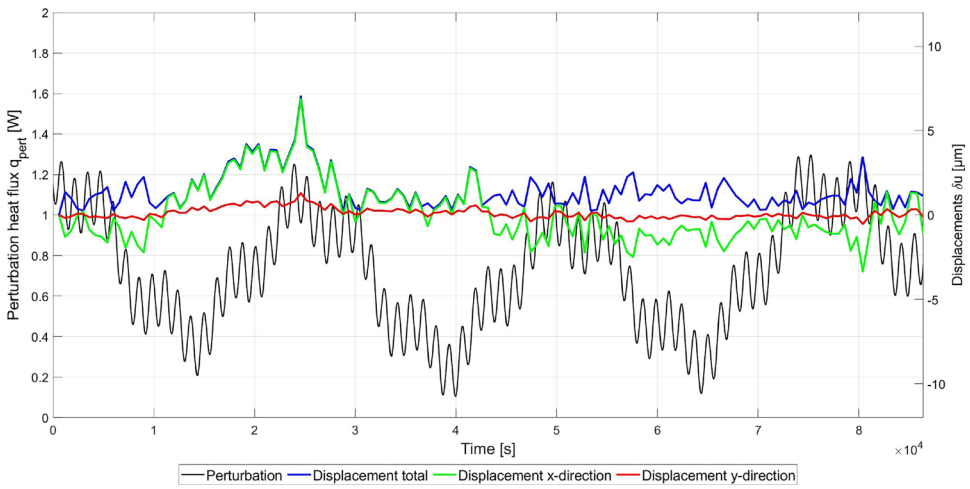

Fig. 25 Displacement, random, $\sigma_T = 0.075$

Looking at Fig. 28, it is very clear that there is a very good compensation of the displacements. The steps in the heating power are almost not visible at all in the displacements. The displacement of the two reference points in y-direction remains almost constant at 0 µm, only displacements in x-directions at an average of ±2 µm up to a maximum of

Table 9 Displacement, random, $\sigma_T = 0.075$ K

Direction	Uncontrolled	Controlled	Difference	Factor
Total	10.36 µm	3.43 µm	6.93 µm	3.02
x	10.15 µm	3.35 µm	6.8 µm	3.03
y	1.63 µm	0.53 µm	1.10 µm	3.08

5 µm can be seen. The total displacement, which results from the vectorial addition of the two components, is about 4 µm.

5 Summary and outlook

In this work, the results from [3] could be confirmed. Furthermore, it could be shown that the revised experimental setup is able to achieve a more efficient structural stabilization with respect to the control performance. Following on from this, an improvement of the measured temperature values is possible by means of a linear compensation function and the approximation of the differences between simulation and sensor measured values to the simulated values leads to further improvements in the structural stability, as well as a significant improvement in the temperature field stabilization.

In a further step, it could be demonstrated that the implemented filter-controller approach is able to compensate displacements caused by randomly superimposed sinusoidal perturbations with improvements in the range of factor 3. Thus, the experimentally determined factors show a clear discrepancy to those from the simulations of [1] in the range of 10–100. However, the causes here are the rudimentary experimental setup, deficits in the measurements of the displacements, and simplifications in the model.

Furthermore, it could be shown that the system can also react to abrupt changes of the heating power by a

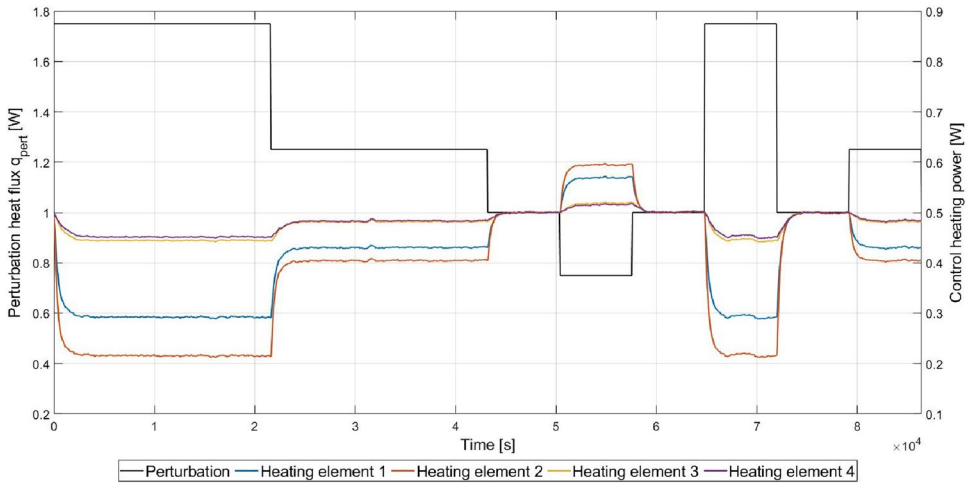

Fig. 26 Control heating power, stepped perturbation

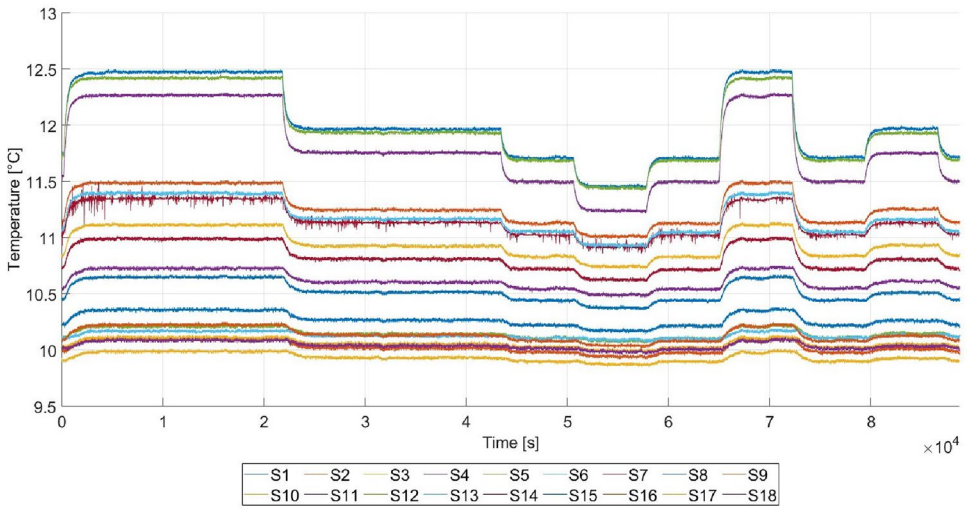

Fig. 27 Temperature curve, stepped perturbation

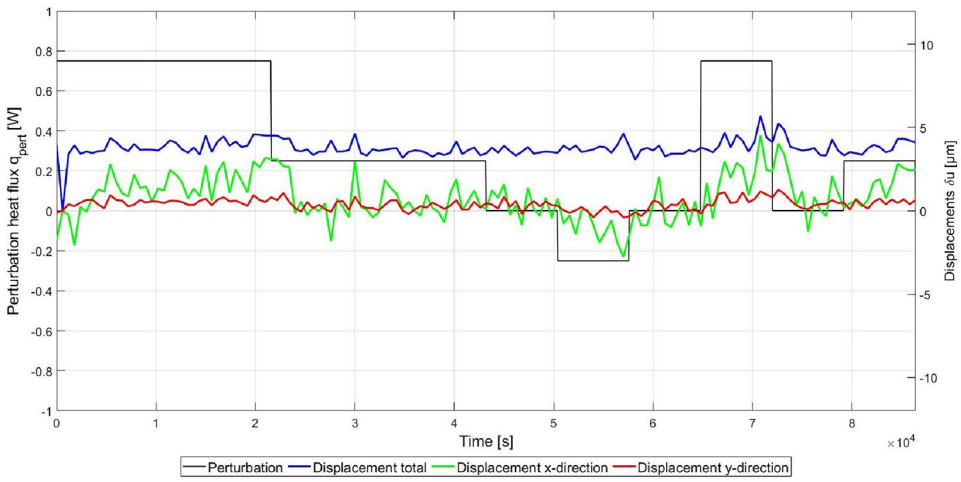

Fig. 28 Displacement, stepped perturbation

step function, and thus, not only periodic changes can be compensated.

Furthermore, there are disadvantages in the here presented and extended method of active structure stabilization. First of all, the dependence of the system on a steady state remains; otherwise, no reference can be given for the state to be stabilized. A determination before mission initiation is only possible through error-prone simulation. Therefore, a phase for collecting the necessary data in a thermally stable flight condition must be scheduled in the mission planning, and measurement errors will occur here. Ultimately, the steady state can be either erroneously simulated or measured. In addition, this procedure initially ties up not only the resource of time but also continuous energy, since the control elements must deliver steady-state heating power to also enable cooling. Otherwise, the heating elements would have to be able to cool actively, which is ruled out by the name.

In the next steps, further improvements of the accuracies of sensors and actuators have to be implemented, as these reduce the potential of the method. In addition, a statistical method should be developed which also allows qualitative statements about the stabilization of the system and thus complements the quantitative results of the absolute and relative displacements. In a further step, the parameters for the filter-controller system can then be analyzed more precisely and, in the area of the dynamics of the filter-controller approach, it can be investigated what influence a change in the controller dynamics has on the quality of the stabilization.

Ultimately, this method can then be combined with a selection of other structure-stabilizing methods, such as "phase change materials" [19, 20] or "meta materials" [21], in an overall structure to identify synergies in the field of smart structures.

Acknowledgements These studies represent experimental demonstrations of a patent-protected method for active structural stabilization (Patent: EP000003502711B1) [2]. No funding was received for conducting this study.

Funding Open Access funding enabled and organized by Projekt DEAL.

Data availability Data sets generated during the current study are available from the corresponding author on reasonable request.

Declarations

Conflict of interest The authors have no competing interests to declare that are relevant to the content of this article.

References

1. Ferrer Gil, E.: Framework for active stabilization of thermomechanical distortions in space structures. Dissertation. Neubiberg: Universität der Bundeswehr München, Januar (2019)
2. Förstner, Roger, Gil, Eloi Ferrer: Method for thermomechanically stabilizing an apparatus, control unit, thermomechanical control system, and apparatus. EP3502711 (A1). (2019)

3. Möller, Florian, et al.: Initial validation of a closed loop filter and controller approach for active stabilization of thermomechanical distortions. In: 73rd International Astronautical Congress (IAC) Paris, France, 18-22 September 2022. (2022)
4. Gleich Aluminiumwerk GmbH. Produktdatenblatt EN AW 7075 Aluminium Walzplatte. https://gleich.de/de/produkte/en-aw-7075
5. Heraeus. Platin-Temperatursensor in Dünnschichttechnik. Ed. by Heraeus. https://cdnreichelt.de/documents/datenblatt/B400/M422_DE.pdf
6. Lichtenberger, R.: Ed. by LIMESS Messtechnik und Software GmbH. Krefeld, (2021). https://www.limess.com/de/produkte/q400-bildkorrelation#documents-downloads
7. LIMESS Messtechnik und Software GmbH. Q400 DIC - Spatially resolved measurement of deformation and strain based on digital image correlation. 2022-07-28T10:15:20.000Z. https://www.limess.com/en/products/q400-digital-image-correlation#measurement-principle (visited on 07/28/2022)
8. Hale, Layton C., Slocum, Alexander H.: Optimal design techniques for kinematic couplings. In: Precision Engineering 25(2), 114-127. (2001) ISSN: 01416359. https://doi.org/10.1016/S0141-6359(00)00066-0
9. Auer Kunststofftechnik GmbH Co. KG, ed. Werkstoffdatenblatt Polytetrafluorethylen (PTFE). http://www.auer-kunststofftechnik.de/pdf/Datenblatt%20PTFE.PDF
10. Warweg, Jannis: Entwurf einer isostatischen Halterung für Thermal-Strukturtests im Vakuum. Studienarbeit. Neubiberg: Universität der Bundeswehr München, Oktober (2020)
11. Messlinger, S.: Zur Temperaturmessung mit Platin- Widerstandsthermometern und Prema 5017 DMM. Ed. by Universität Bayreuth. Bayreuth, (2013). https://epub.uni-bayreuth.de/43/1/tmeas-dossier.pdf
12. León, F. Puente: Messtechnik: Grundlagen, Methoden und Anwendungen. 11. Auflage 2019. Berlin: Springer Vieweg, (2019). ISBN: 3662597667
13. Bastamedia. Experten-Lösungen für Mess-, Prüfund Auswerteaufgaben. 7.02.2022. https://www.measx.com/de/ (visited on 02/07/2022)
14. Telemeter Electronic GmbH. Ed. by Telemeter Electronic GmbH. Donauwörth, (2021). https://telemeter.info/de/temperaturmanagement/heizfolien/heizfolien/kapton-heizfolien
15. Lohninger, H.: Fundamentals of Statistics: Optimization Methods - Brute Force Approach. http://www.statistics4u.com/fundstat_eng/cc_optim_meth_brutefrc.html
16. Maschino, Lukas: Kalibrierung und Validierung von Thermal-Vakuumtests zur Identifikation der thermooptischen Eingenschaften eines Satellitenmodells zur Strukturstabilisierung. Masterarbeit. Universität der Bundeswehr München, (2021)
17. Papageorgiou, M., Leibold, M., Buss, M.: Optimierung. Berlin, Heidelberg: Springer Berlin Heidelberg, (2012). ISBN: 978-3-540-34012-6. https://doi.org/10.1007/978-3-540-34013-3
18. Engineering Toolbox. Emissivity Coefficients common Products. (2003). https://www.engineeringtoolbox.com/emissivitycoefficients-d_447.html
19. Wild, Dominik., et al.: Thermal Characterization of additive manufactured Integral Structures for Phase Change Applications. 2020 International Conference on Environmental Systems, (2020). https://ttu-ir.tdl.org/handle/2346/86394
20. Wild, Dominik, Czupalla, Markus, Foerstner Roger: Modeling, Prediction and Test of Additive Manufactured Integral Structures with Embedded Lattice and Phase Change Material Applying Infused Thermal Solutions (ITS). 50th International Conference on Environmental Systems, (2021). https://ttu-ir.tdl.org/handle/2346/87104
21. Buchmann, Erhard., et al.: A Unit Cell with Tailorable Negative Thermal Expansion Based On a Bolted Additively Manufactured Auxetic Mechanical Metamaterial Structure: Development and Investigation. In: Proceedings of the Munich Symposium on Lightweight Design 2021. (2021), pp. 198-211